THEORETICAL CHEMISTRY INSTITUTE

THE UNIVERSITY OF WISCONSIN

MOLECULAR COLLISIONS. XVI. COMPARISON OF GPS WITH CLASSICAL TRAJECTORY CALCULATIONS OF ROTATIONAL INELASTICITY FOR THE Ar-N_2 SYSTEM

M. D. Pattengill, R. A. La Budde, R. B. Bernstein and C. F. Curtiss

WIS-TCI-441

18 June 1971

MADISON, WISCONSIN

MOLECULAR COLLISIONS. XVI. COMPARISON OF GPS WITH CLASSICAL TRAJECTORY CALCULATIONS OF ROTATIONAL INELASTICITY FOR THE Ar-N_2 SYSTEM *

by

M. D. Pattengill, R. A. La Budde, R. B. Bernstein and C. F. Curtiss

Theoretical Chemistry Institute and Chemistry Department

University of Wisconsin, Madison, Wisconsin 53706

ABSTRACT

The classical limit of the "infinite order" generalized phase shift (GPS) treatment of rotationally inelastic atom-molecule collisions was put into computationally feasible form in paper XV of this series. It is now applied to a model problem intended to approximate thermal scattering of the Ar-N_2 system (collisional energy of $\frac{3}{2}$ kT at 300°K), at the same time comparing its predictions with exact classical trajectory (CT) results. This comparison indicates that the present version of the GPS method overestimates the rotational excitation and underestimates the de-excitation, while maintaining the total inelasticity at approximately the correct (CT) value. An approximate "quantization"

---

* This research was supported by Grants GP-12832 and GB-16665 from the National Science Foundation and Grant NGL 50-002-001 from the National Aeronautics and Space Administration.

of the classical results leads to an estimate of the quantal cross sections corresponding to changes by ± 2, ± 4 and ± 6 from an initial rotor quantum state $\overline{\ell} = 10$. It is found that most of the total inelastic cross (of some 32 $\mathring{A}^2$) arises from the first-order-allowed transitions ($\Delta\ell = \pm 2$).

In paper XV of this series,[1] the classical limit of the so-called "infinite order" approximation[2] of the generalized phase shift (GPS) treatment[3] of rotational inelasticity was applied to the case of atom-rigid rotor scattering. The method of calculation consisted of generating a specified arbitrary number of moments of the rotational inelasticity probability density function $\mathcal{P}(\Delta E_{rot})$ at various impact parameters b . Inversion of a given set of moments then yielded $\mathcal{P}(\Delta E_{rot})$ as a function of b . These curves could then be integrated over b to obtain rotational inelasticity cross sections $d\mathcal{Q}(\Delta E_{rot})/d(\Delta E_{rot})$ as functions of ΔE_{rot} .

Although paper XV demonstrated the computational feasibility and economy of the classical GPS treatment and established that it predicts qualitatively correct trends, it was not possible to assess the accuracy of the approximations inherent in the method. One purpose of the present paper is to provide such an assessment.

Utilizing a model anisotropic interaction potential, $V(r, \theta)$, chosen to simulate the Ar-N_2 system, scattering results are calculated at "thermal" conditions using the classical limit of the "infinite order" GPS treatment. These results are then compared with those obtained from an exact classical trajectory (CT) Monte Carlo study for the same case. The comparison thus obtained serves as a direct test of the validity of the approximations entering the present version of the GPS treatment, the principal one being that of a curved, planar trajectory governed by the central (orientation-averaged) portion of the anisotropic interaction potential.

In Section I, the interaction potential and parameters chosen for the Ar-N_2 system are discussed; in Section II, the computational procedures are described. Section III presents a comparison of results obtained from the GPS and CT studies. Comments and conclusions regarding the validity of the GPS method are summarized in Section IV. In addition, results obtained from the first-order approximation of the semiclassical limit of the GPS treatment (as described in paper XIV of this series[4]) are presented in the Appendix.

The overall purpose of this paper is twofold. First, as noted above, it serves as a direct comparison of the GPS approximation method with the exact CT results for the same model problem. Second, it is an attempt at predicting realistic rotational inelasticity cross sections for an experimentally accessible system, viz., the scattering of Ar by N_2.

I. INTERACTION POTENTIAL AND Ar-N_2 PARAMETERS

The interaction potential chosen to represent the Ar-N_2 system is the simplest one consistent with the available information on this atom-molecule pair. It consists of a Lennard-Jones (12,6) central potential with $r^{-12}\,P_2(\cos\theta)$ repulsive and $r^{-6}\,P_2(\cos\theta)$ attractive anisotropies:

$$V(r,\theta) = \frac{C_{12}}{r^{12}}\left[1 + b_2 P_2(\cos\theta)\right] - \frac{C_6}{r^6}\left[1 + a_2 P_2(\cos\theta)\right] \tag{1}$$

As usual, r is the Ar-N_2 c.m. separation, θ is the angle between the line joining the centers of mass and the N_2 axis, and $P_2(x)$

is the Legendre polynomial. In addition, $C_{12} = 4\epsilon\sigma^{12}$ and $C_6 = 4\epsilon\sigma^6$, where ϵ and σ are, respectively, the usual L-J(12,6) well-depth and size parameters.

Estimated values used for the parameters in Eq. (1) were[5]: $\epsilon = 1.65\ (\pm 0.05) \times 10^{-14}$ erg, $\sigma = 3.5\ (\pm 0.1) \times 10^{-8}$ cm., $a_2 = 0.13\ (\pm 0.01)$ and $b_2 = 0.5 \begin{pmatrix} +\ 0.2 \\ -\ 0.1 \end{pmatrix}$. The value of ϵ is taken from a recent analysis of molecular beam scattering data.[6] The size parameter σ is estimated from molecular beam scattering data[6] and transport properties.[7] The attractive anisotropy parameter a_2 is taken from the polarizability anisotropy[8] of N_2. All these quantities are rather well-known. Unfortunately, the repulsive anisotropy parameter b_2 is quite uncertain, yet it plays a strong role in the predicted inelastic scattering. The value used for b_2 was based on a modification of the well-known "dumbbell-model".[9] The rotational constant for N_2, $B_e = 2.010\ cm^{-1}$, and its equilibrium bond length, $r_e = 1.094 \times 10^{-8}$ cm, were taken from Herzberg.[10] Using these quantities one obtains $\Lambda^* = 0.1993$ for the deBoer quantum parameter and $M\sigma^2/I = 24.07$ for the moment of inertia parameter.[1]

For the present computations, the initial translational energy, E_{trans}, and rotational energy, E_{rot}, were taken to be the average classical values at 300°K. Thus, $E_{trans} = \frac{3}{2}kT = 6.212 \times 10^{-14}$ erg and $E_{rot} = kT = 4.141 \times 10^{-14}$ erg.

II. COMPUTATIONAL PROCEDURES

The computational procedures employed to obtain rotational inelasticity probability density functions by the GPS method were identical

to those used in paper XV. For each set of initial conditions, i.e., for given E_{trans}, E_{rot}, and b, the required generalized action integrals $S^{(2)}_{n,\alpha,s}$ were evaluated as described in paper XIV. The first ten moments M_n ($n = 1, \ldots, 10$) of the density function were then calculated from[11] Eq. (XV. C1) by use of the 16,000 point method of optimal coefficients quadrature. Inversion of the moments was accomplished by the Gram-Charlier technique (cf. Eqs. (XV. 29) and (XV. 30)). As in paper XV, convergence tests established the validity of the moments to about 3 significant figures and the "inverted" density function curves to better than about 10%.

For the exact CT Monte Carlo computations, the classical equations of motion were integrated, by techniques described elsewhere,[12] to an accuracy of 3 or 4 figures in the coordinates and momenta. Initial conditions for the trajectories were selected by use of a set of number theoretical lattice points.[13] Depending on the impact parameter, batches of either 98, 135 or 222 trajectories were used in the determination of the moments of the density functions. Convergence tests indicated that the integrations over the trajectories to obtain the moments were at least as accurate as the trajectories themselves (i.e., validity to 3 or 4 figures). As for the GPS results, inversion of the first ten CT moments was carried out by the Gram-Charlier technique.

For both the GPS and CT methods, integrations of the density function curves over b to obtain cross sections were performed graphically (density curves had been computed at increments in $b^*(= b/\sigma)$ of 0.1 over the range $0.3 \leq b^* \leq 1.3$) with a resulting accuracy of a few percent.

III. RESULTS AND DISCUSSION

Values obtained for the second through the sixth moments (M_2-M_6) of the rotational inelasticity probability density functions are plotted vs. b^* in Fig. 1; here Fig. 1(a) illustrates the GPS calculations and 1(b) the CT results. As expected, the moments rapidly approach zero for large b^*. At moderate and small impact parameters ($b^* \lesssim 1.0$), the GPS method consistently overestimates the magnitudes of the moments. It should be noted that while the GPS moments are all positive, the CT values for the odd moments, M_3 and M_5, are negative. Fig.2 presents comparative plots of M_1 and M_2 showing the rather marked discrepancy between the GPS and CT results at low b^*.

Fig. 3 shows probability density functions[1] $\mathcal{P}(\Delta f)$ at $b^* = 0.3$ and 1.0 (as in paper XV, $\Delta f = \Delta E_{rot}/E_{trans}$ is the fractional energy transfer) obtained in three different ways. First, CT histograms, which establish directly the rotational inelasticity probability density function $\mathcal{P}(\Delta f)$, are shown. Second, a curve (labelled CT), which was obtained by inversion of the first ten CT moments, is superimposed. The results in Figs. 3(a) and 3(b) correspond respectively to 222 and 135 total trajectories (histogram intervals have approximately equal statistical weights). It is apparent that $\mathcal{P}(\Delta f)$ curves obtained from the CT moment inversions provide quite accurate representations of the histogram data. This agreement attests to the accuracy of the Gram-Charlier moment inversion technique. Third, for comparison, probability density function curves obtained by inversion of the first ten GPS moments are shown.

$\mathcal{P}(\Delta f)$ curves for various b^* obtained by both the GPS and CT methods are displayed in Fig. 4. (As usual, the $\mathcal{P}(\Delta f)$ curves were obtained by inversions of the first ten moments.) Fig. 4(a) shows the GPS and 4(b) the CT results. The GPS curves deviate from the CT ones mainly by their persistence to large positive values of Δf (rotational excitation).

Also shown in Fig. 4 are representative plots of $2\pi b\,\mathcal{P}$ vs b for various values of Δf, the left and right panels corresponding to de-excitation and excitation respectively. As in Paper XV, the partial inelastic contribution to the total cross section is defined:

$$\frac{d\,Q(\Delta f)}{d(\Delta f)} = 2\pi \int_0^\infty b\,\mathcal{P}\,db \qquad (2)$$

so that the total inelastic cross section for energy transfer exceeding some minimum value of $|\Delta f_1|$ is given by:

$$Q(|\Delta f| > |\Delta f_1|) = \left| \int_{\Delta f_1}^{\Delta f_2} \frac{d\,Q(\Delta f)}{d(\Delta f)}\, d(\Delta f) \right| \qquad (3)$$

where Δf_2 is determined by the energy conservation limit. The area under each such curve of $2\pi b\,\mathcal{P}$ vs b thus gives $\frac{dQ(\Delta f)}{d(\Delta f)}$ in units of $\mathring{A}^2$. Fig. 5 presents these integrals, $\frac{dQ(\Delta f)}{d(\Delta f)}$, as functions of Δf. To be noted is the "tail" of the GPS curve extending to high Δf.

Integrated values of the curves in Fig. 5 as functions of the lower limit Δf_1 (cf. Eq. (3)) are shown[14] in Fig. 6. Thus, having specified a value of Δf_1, the total inelastic cross section for energy transfer

greater than this lower limit can be obtained directly from the ordinates of the curves[15] in Fig. 6. Consistent with the preceding results of Fig. 5, and regardless of the choice of Δf_1, the GPS method overestimates the cross section for positive Δf (rotational excitation) and underestimates it for negative Δf (rotational de-excitation).

All the results described thus far are of a purely classical nature. Nowhere has the concept arisen of a direct state-to-state transition probability or cross section. For purposes of obtaining an impression of the importance of the deviations of the GPS from the CT results, however, it is interesting to attempt to "quantize" the results, even though the correspondence is not rigorous (however, based on the work of Miller[16] and Marcus[17] a well-defined classical correspondence can be established).

For quantal rotor scattering, the initial N_2 rotational energy used in the present calculations would correspond to an initial quantum number $\bar{\ell}$ of 9.69. In the classical treatment, only the product of $\bar{\ell}$ with the deBoer quantum parameter $\Lambda^*(= h/\sigma\sqrt{2M\varepsilon})$ enters the problem. Thus, it is convenient to change Λ^* slightly (i.e., reduce it by some 3%) so as to make $\bar{\ell}$ an integer, i.e., 10. (This slight alteration in Λ^* would correspond to varying the L-J (12,6) parameters slightly.) One may then calculate Δf values corresponding to integer changes in the rotational quantum number. In anticipation of this analysis, such "quantized" values of Δf have been indicated by marks on the abscissae of Figs. 4-6. Moreover, since by symmetry only even $\Delta\ell$ changes are allowed for N_2, it is assumed that the cross section

for a specified $\Delta\ell$ change is given by integrating $\frac{dQ(\Delta f)}{d(\Delta f)}$ between Δf values corresponding to the odd quantum numbers which bracket the even final number (i.e., the cross section for a $10 \to 8$ transition is obtained by integrating between states 7 and 9, etc.). The inner region near $\Delta f = 0$ corresponding to $9 < \ell < 11$ is considered elastic scattering.

For the present problem, this procedure leads to essentially four allowed de-excitation and three allowed excitation channels for N_2. The results obtained from Fig. 6 are summarized in Table 1.

Adding together the contributions from excitation and de-excitation leads to a total inelastic cross section[18] of 33.2Å^2 for the GPS method compared to 31.4 from the CT results. In the Appendix a comparison is made with the first-order semiclassical GPS prediction of this quantity.

IV. SUMMARIZING DISCUSSION

The twofold purpose of this paper has been mentioned in the Introduction. With regard to the assessment of the GPS approximation, it is hoped that the results presented here for the model problem are typical of the accuracy which may be expected from the classical limit of the "infinite order" GPS treatment of rotational inelasticity, using the linearized expression for the generalized phase shift given by Eq. (XII.72). As is evident from Figs. 4-6, this approximation of the GPS method consistently favors excitation at the expense of de-excitation. Any attempt to categorize the GPS approximation is complicated by the many levels at which comparison with the exact CT results may be made. If attention is restricted to the observables,

TABLE 1. "Quantized" Rotational Transition Cross Sections ($\mathring{A}^2$)

De-excitation:			Excitation:		
$Q(\bar{\ell} \rightarrow \ell)$	GPS	CT	$Q(\bar{\ell} \rightarrow \ell)$	GPS	CT
$10 \rightarrow 8$	11.7	13.2	$10 \rightarrow 12$	9.8	9.6
$10 \rightarrow 6$	3.3	4.8	$10 \rightarrow 14$	4.8	1.0
$10 \rightarrow 4$	0.8	2.2	$10 \rightarrow 16$	2.0	0.0
$10 \rightarrow 2$	0.6	0.6			
Total	16.4	20.8	Total	16.8	10.6

Total Inelastic Cross Section:

GPS	CT
33.2	31.4

i.e., cross sections, predicted by the theory, the situation is not clear-cut. Although the $Q(|\Delta f|>|\Delta f_1|)$ curves for the GPS and CT methods presented in Fig. 6 differ significantly, the total inelastic cross section is well-predicted by the GPS method. In addition, considering the present level of uncertainty in knowledge of atom-molecule interaction potentials, the comparison obtained for the "quantized" cross sections (Table 1) is perhaps encouraging. It is to be expected, however, that an exact application of the GPS method[3] of Paper XII, using the full expression for the generalized phase shift, Eq. XII-89, would lead to results identical with the CT results. More exact computational applications of these methods will be considered in later papers.

With regard to the problem of prediction of "observable" inelastic cross sections for an actual system it is believed that until further and more accurate information on the interaction potential for the $Ar-N_2$ system becomes available, the present (CT) calculations are to be considered of predictive, if only semi-quantitative, value.

APPENDIX

It is of interest to consider the predictions of the first-order semiclassical GPS treatment for Ar-N_2. As given by Eq. (XIV.13), the first-order transition probability for an interaction potential containing a pure $P_2(\cos\Theta)$ anisotropy, $P_{\bar{\lambda}}^{(1)}(\bar{\ell};\bar{\ell}\pm 2)$, is a simple combination of the generalized action integrals (which are required in the "infinite order" classical GPS treatment). Fig. 7 presents a plot of $P_{\bar{\lambda}}^{(1)}(\bar{\ell};\bar{\ell}\pm 2)$ obtained via Eq. (XIV.13) vs b^* (In all calculations presented in the Appendix, Λ^* has been set equal to that (0.1933) used in the "quantized" version of the classical results.) It has been shown[19] that for large b^* (i.e., weak coupling) the following relationship exists between $P_{\bar{\lambda}}^{(1)}(\bar{\ell};\bar{\ell}\pm 2)$ and the second moment of the "infinite order" classical GPS rotational inelasticity probability density function M_2 :

$$P_{\bar{\lambda}}^{(1)}(\bar{\ell};\bar{\ell}\pm 2) = \frac{\pi^4 E^{*2}}{2\Lambda^{*2}\jmath^2} M_2 \qquad \text{(A1)}$$

where E^* ($= E_{trans}/\varepsilon$) is the reduced initial translational energy and $\jmath$ is defined by Eq. (XIV.27). Values of $P_{\bar{\lambda}}^{(1)}(\bar{\ell};\bar{\ell}\pm 2)$ obtained from Eq. (A1) are also presented in Fig. 7. The extent of agreement between the two calculations at low impact parameter is somewhat surprising (however, see Footnote 11 of Paper XV.)

It is also of interest to attempt to estimate the total inelastic cross section from the first-order transition probability, following the approximation of Fenstermaker and Bernstein[20]. Thus, in Fig. 8,

the sum $P_{\lambda}^{(1)}(10;\ 8) + P_{\lambda}^{(1)}(10;\ 12)$ (i.e., $2P_{\lambda}^{(1)}(\bar{\ell};\bar{\ell} \pm 2)$) is plotted vs. πb^2. This transition probability sum attains a value of 0.5 at a πb^2 of about 43Å^2. This gives a first-order estimate of the total inelastic cross section, which is seen to be about 25% in excess of the correct value (cf. Table 1).

FOOTNOTES

1. M. D. Pattengill, C. F. Curtiss and R. B. Bernstein, Wisc. Theor. Chem. Inst. Rept. WIS-TCI-436, 16 April 1971 (submitted to J. Chem. Phys.).
2. See Footnote 5 of Reference 1 for a definition of this designation.
3. C. F. Curtiss, J. Chem. Phys. 52, 4832 (1970), paper XII of this series.
4. M. D. Pattengill, C. F. Curtiss and R. B. Bernstein, J. Chem. Phys. 54, 2197 (1971), paper XIV of this series.
5. Numbers in parentheses indicate the estimated accuracy of the estimates.
6. K. G. Anlauf, R. W. Bickes, Jr., and R. B. Bernstein, J. Chem. Phys. 54, 3647 (1971).
7. F. W. Reiter, Ber. Bunsen. Gesell., 74, 562 (1970).
8. N. J. Bridge and A. D. Buckingham, Proc. Roy Soc. A295, 334 (1966).
9. For a recent application, see, e.g., P. G. Burke, D. Scrutton, J. H. Tait and A. J. Taylor, J. Phys. B, 2, 1155 (1969). Briefly, the procedure employed in the present work was as follows: The dumbbell-model was used to calculate b_2 values for both Ar-N_2 and He-H_2 at r = σ . A "correction factor" was then defined by taking the ratio of the dumbbell b_2 for He-H_2 to that obtained from the *ab initio* calculation of the He-H_2 interaction potential by M. D. Gordon and D. Secrest (J. Chem. Phys. 52, 120 (1970)). This factor was applied to the above-estimated dumb-bell b_2 for Ar-N_2.

10. G. Herzberg, Spectra of Diatomic Molecules, Van Nostrand, New York, 1950.

11. Eq. (XV.C1) denotes Eq. (C1) of paper XV of this series, etc.

12. R. A. La Budde and R. B. Bernstein, Wisc. Theor. Chem. Inst. Rept. WIS-TCI-433 (in preparation; to be submitted to J. Chem. Phys.).

13. For a discussion of the theory of this method see N. M. Korobov, Sov. Math. Dokl. 1, 696 (1960). The quadrature points were calculated to maximize the trigonometric degree of the formula.

14. For the sake of consistency, the small "tails" of the $\frac{dQ(\Delta f)}{d(\Delta f)}$ curves extending past the conservation limits have been included in the integrals.

15. Of course, $Q(|\Delta f_2|>|\Delta f_1|)$ for arbitrary $|\Delta f_2|$ may be obtained by simply taking the difference between the appropriate two points on the curve.

16. W. H. Miller, J. Chem. Phys. 53, 1949 (1970).

17. R. A. Marcus, J. Chem. Phys. 54, 3965 (1971).

18. It is interesting to note that the results obtained here are not inconsistent with the total inelastic cross section of ca. 75Å^2 obtained from the dominant coupling approximation for Ar-N_2 by R. B. Bernstein, A. Dalgarno, H. Massey and I. C. Percival, Proc. Roy. Soc. A274, 427 (1963), if one takes into account that their assumed interaction potential was more anisotropic ($a_2 = 0.16$, $b_2 = 0.7$).

19. C. F. Curtiss (unpublished notes).

20. R. W. Fenstermaker and R. B. Bernstein, J. Chem. Phys. 47, 4417 (1967).

FIGURE LEGENDS

Figure 1. $M_2, M_3 \ldots, M_6$ vs b^*. (a) GPS, (b) CT. Note that in (b), $-M_3$ and $-M_5$ have been plotted.

Figure 2. Comparison of M_1 and M_2 values obtained by the GPS and CT methods. (a): M_1, (b): M_2.

Figure 3. Comparison of CT histograms for $\mathcal{P}(\Delta f)$ with curves obtained by inversions of the first ten CT and GPS moments of $\mathcal{P}(\Delta f)$. (a): $b^* = 0.3$, (3): $b^* = 1.0$. Energy conservation limits are given by marks on the abscissae at $\Delta f = -0.67$ and $+1.0$.

Figure 4. $\mathcal{P}(\Delta f)$ vs Δf obtained by inversions of the first ten moments for various b^*. Insets give $2\pi b\,\mathcal{P}(\Delta f)$ in $\mathring{A}$ vs $b(\mathring{A})$ for the indicated values of Δf. (a) GPS (b) CT. Marks at $\Delta f = -0.67$ and 1.0 give energy conservation limits. Marks at $\Delta f = \ldots, -0.35, -0.24, -0.13, 0, 0.14, 0.30, 0.46, \ldots$ etc. denote Δf values corresponding to transitions from $\bar{\ell} = 10$ to rotor states with quantum numbers ℓ of $\ldots, 7, 8, 9, 10, 11, 12, 13, \ldots$ etc. at $\Lambda^* = 0.1933$.

Figure 5. $\frac{dQ(\Delta f)}{d(\Delta f)}$ in $\mathring{A}^2$ vs Δf from the GPS and CT methods. Markings on abscissa identical to Fig. 4.

Figure 6. $Q(|\Delta f| > |\Delta f_1|)$ in $\mathring{A}^2$ vs Δf from the GPS and CT methods. Markings on abscissa identical to Figs. 4, 5.

Figure 7. $P_\lambda^{(1)}(\bar{\ell};\bar{\ell} \pm 2)$ from Eqs. (XIV.27) and (A1) vs. b^*.

Figure 8. $P_\lambda^{(1)}(10;8) + P_\lambda^{(1)}(10;12)$ equal to $2P_\lambda^{(1)}(\bar{\ell};\bar{\ell} \pm 2)$ vs. $\pi b^2\,(\mathring{A}^2)$.

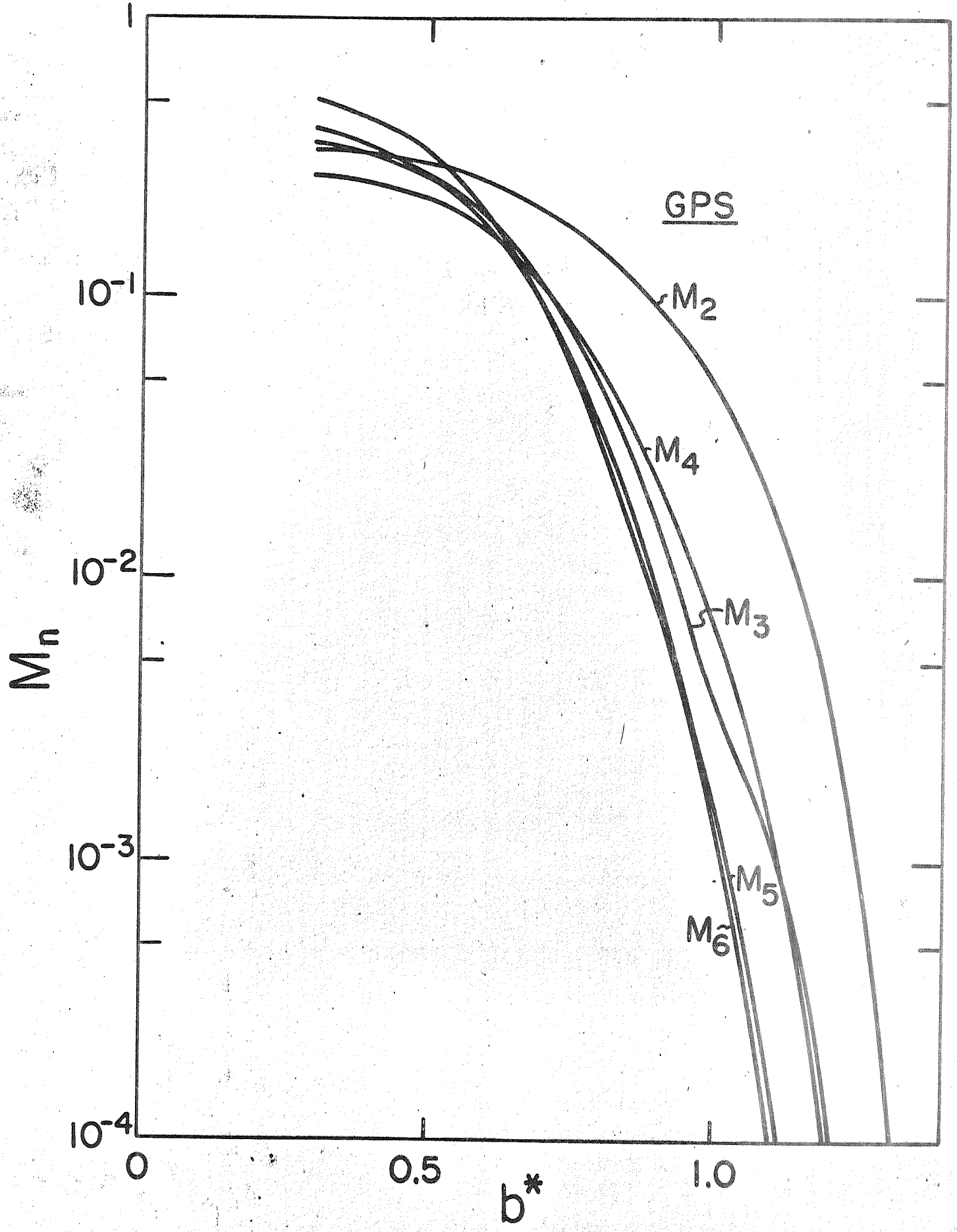

Figure 1a

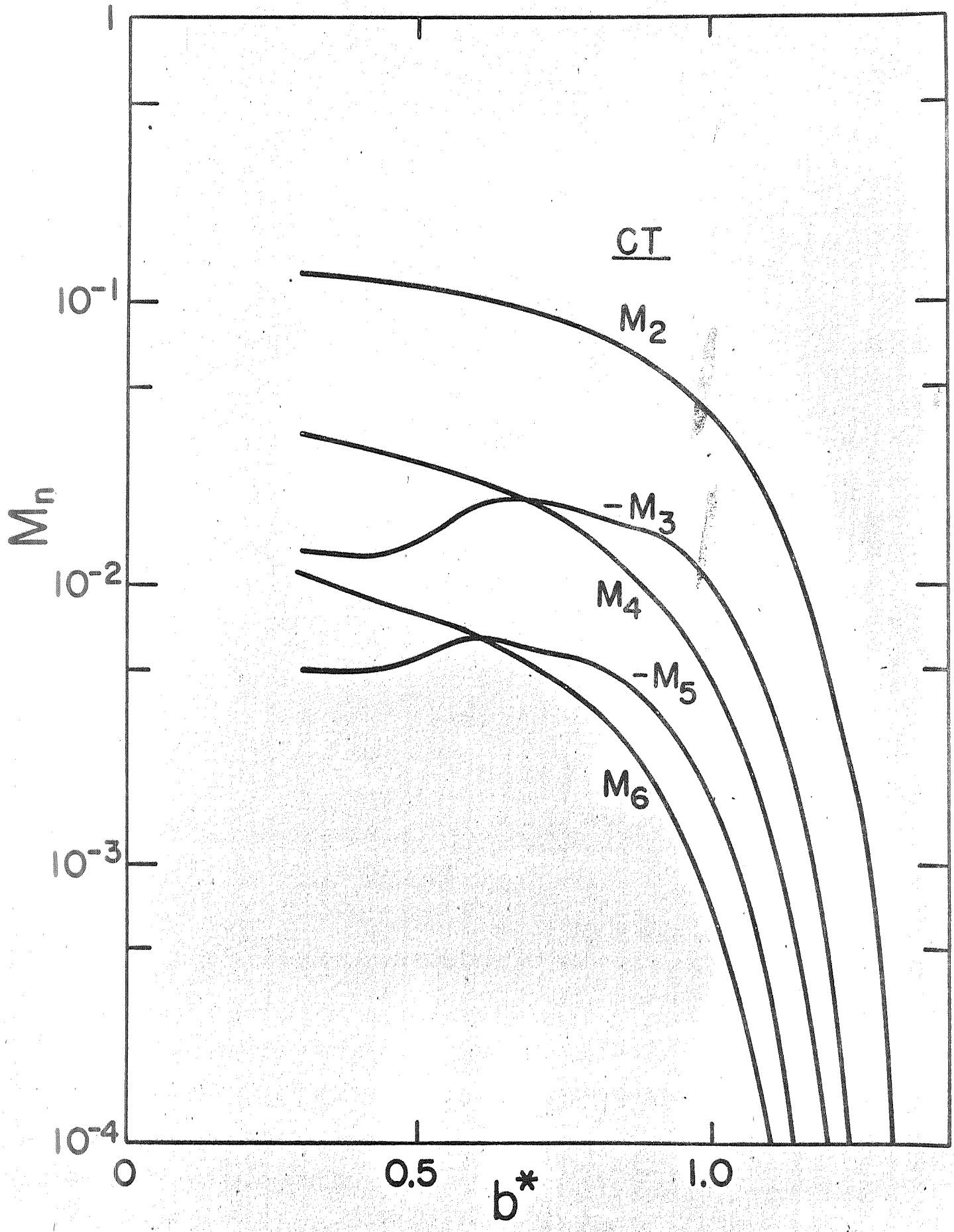

Figure 1b

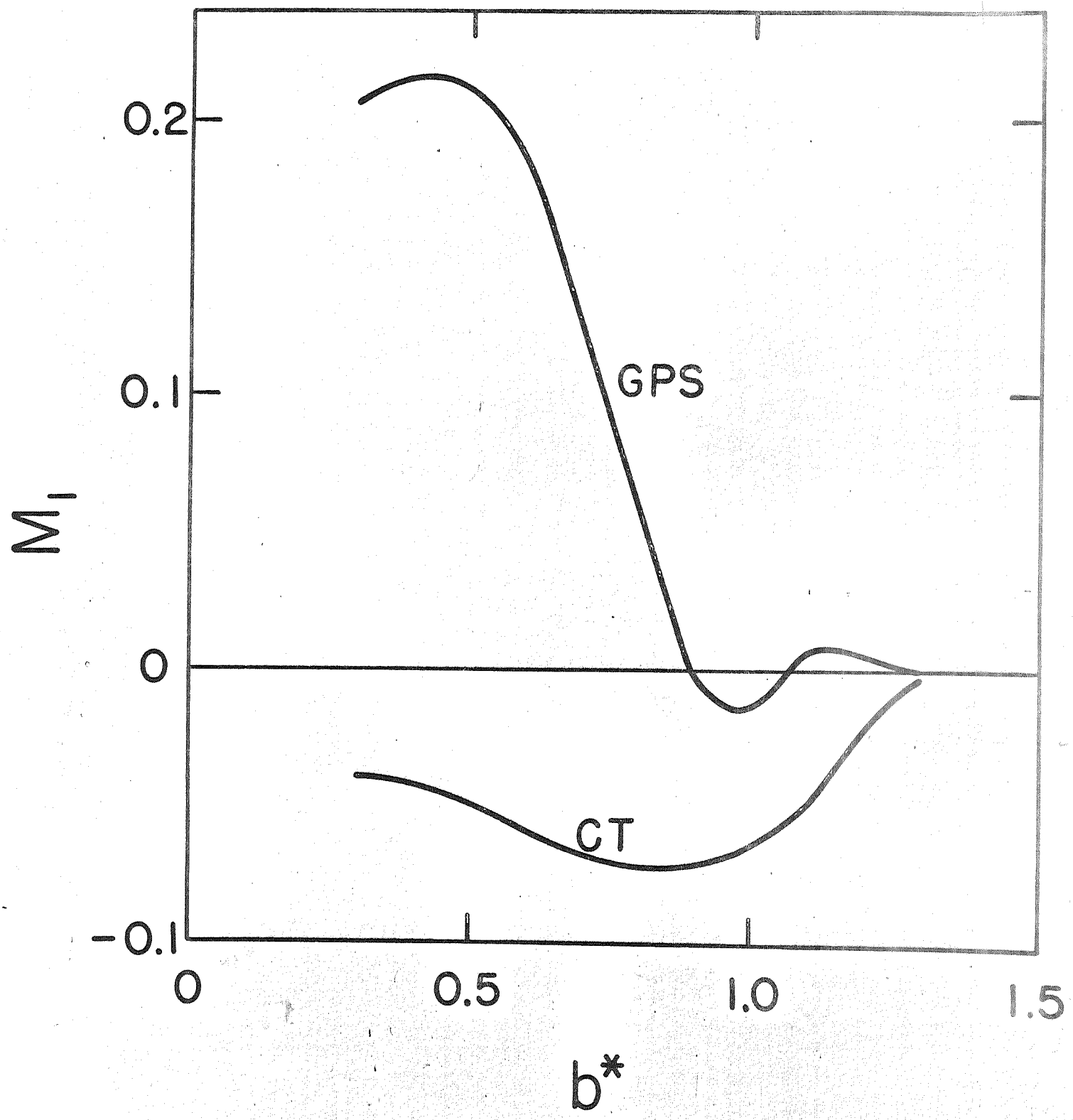

Figure 2a

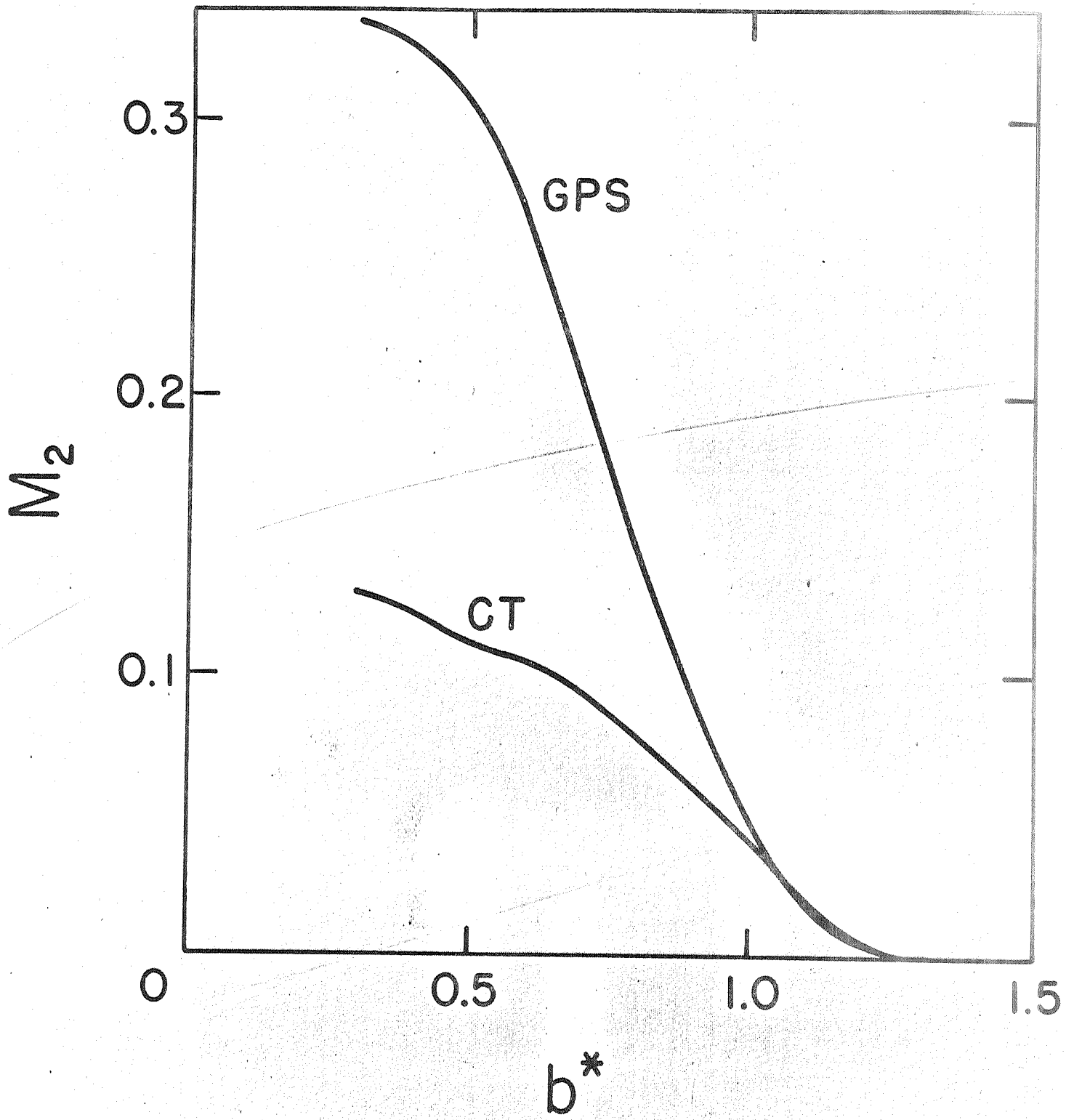

Figure 2b

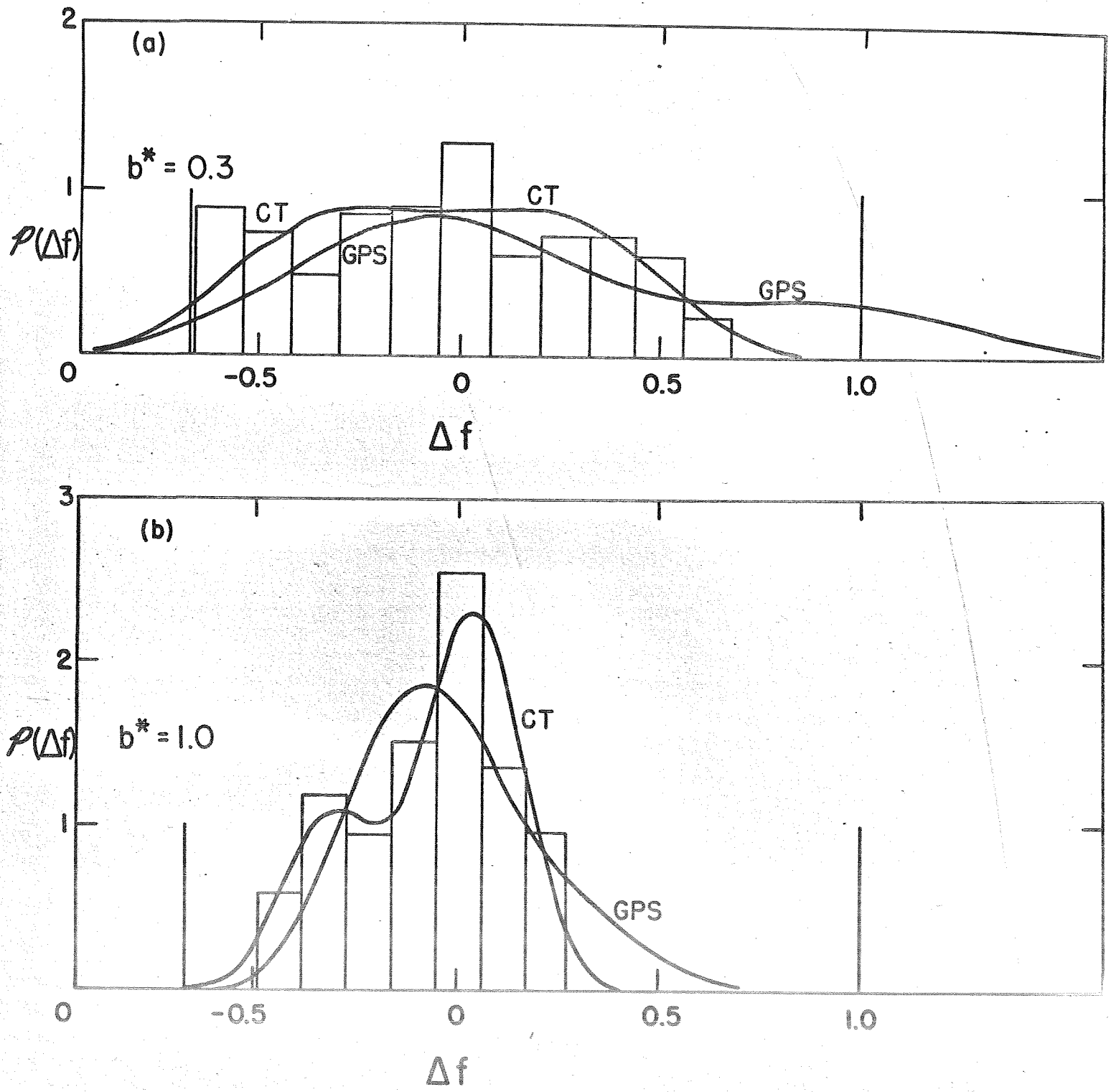
(a)
b* = 0.3
CT
CT
GPS
GPS
P(Δf)
2
1
0
-0.5
0
0.5
1.0
Δf
(b)
b* = 1.0
CT
GPS
P(Δf)
3
2
1
0
-0.5
0
0.5
1.0
Δf

Figure 3

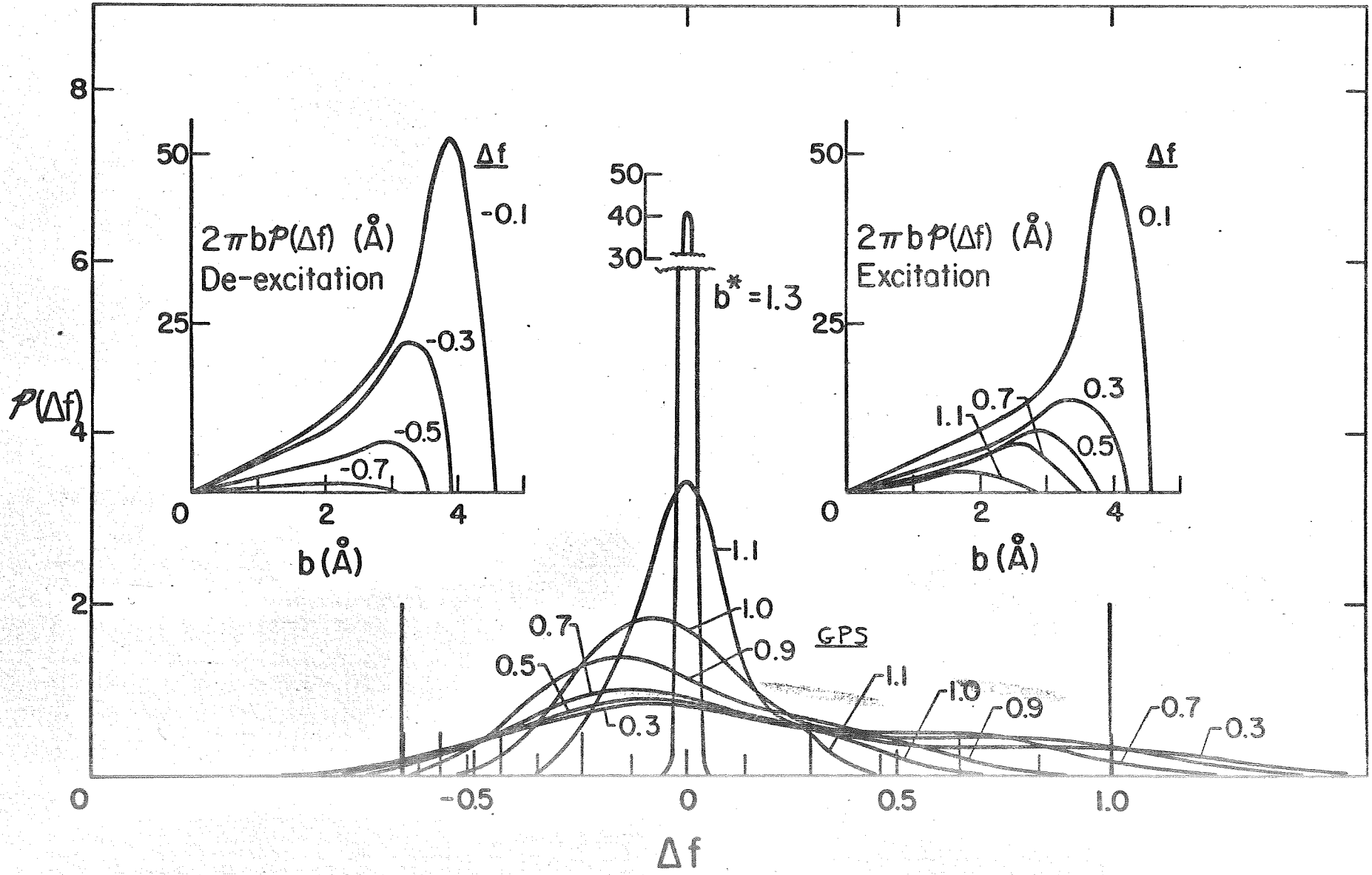
8
6
4
2
0
P(Δf)
50
25
0
2
4
b(Å)
2πbP(Δf) (Å)
De-excitation
Δf
-0.1
-0.3
-0.5
-0.7
50
40
30
b* = 1.3
1.1
1.0
0.9
0.7
0.5
0.3
GPS
2πbP(Δf) (Å)
Excitation
0.1
0.7
0.3
0.5
1.1
-0.5
0
0.5
1.0
Δf

Figure 4a

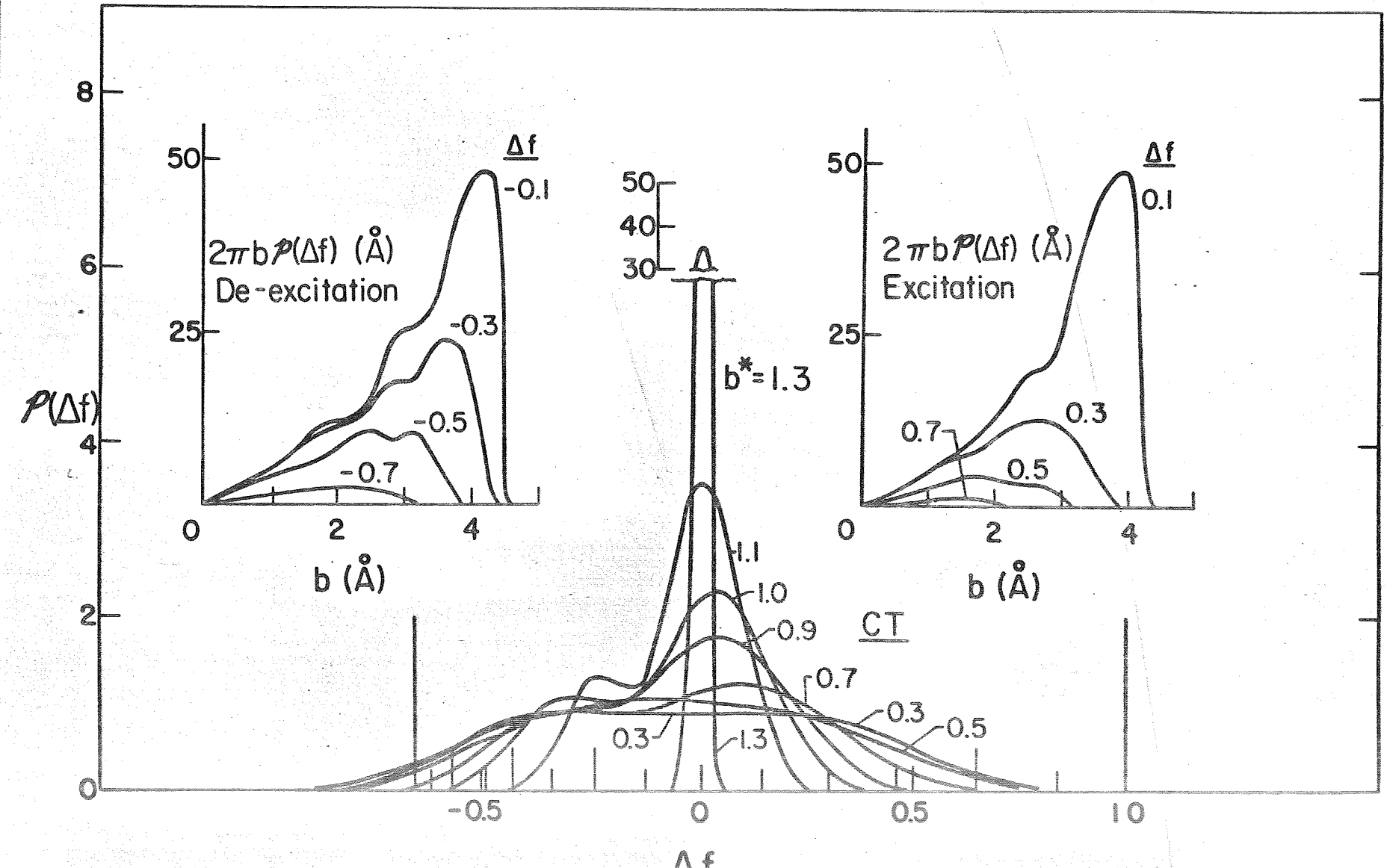
P(Δf)
8
6
4
2
0
-0.5
0
0.5
1.0
Δf
CT
b*=1.3
1.1
1.0
0.9
0.7
0.3
0.5
0.3
1.3
50
40
30
Δ
2πbP(Δf) (Å)
De-excitation
Δf
-0.1
-0.3
-0.5
-0.7
50
25
0
2
4
b (Å)
2πbP(Δf) (Å)
Excitation
Δf
0.1
0.7
0.3
0.5
50
25
0
2
4
b (Å)

Figure 4b

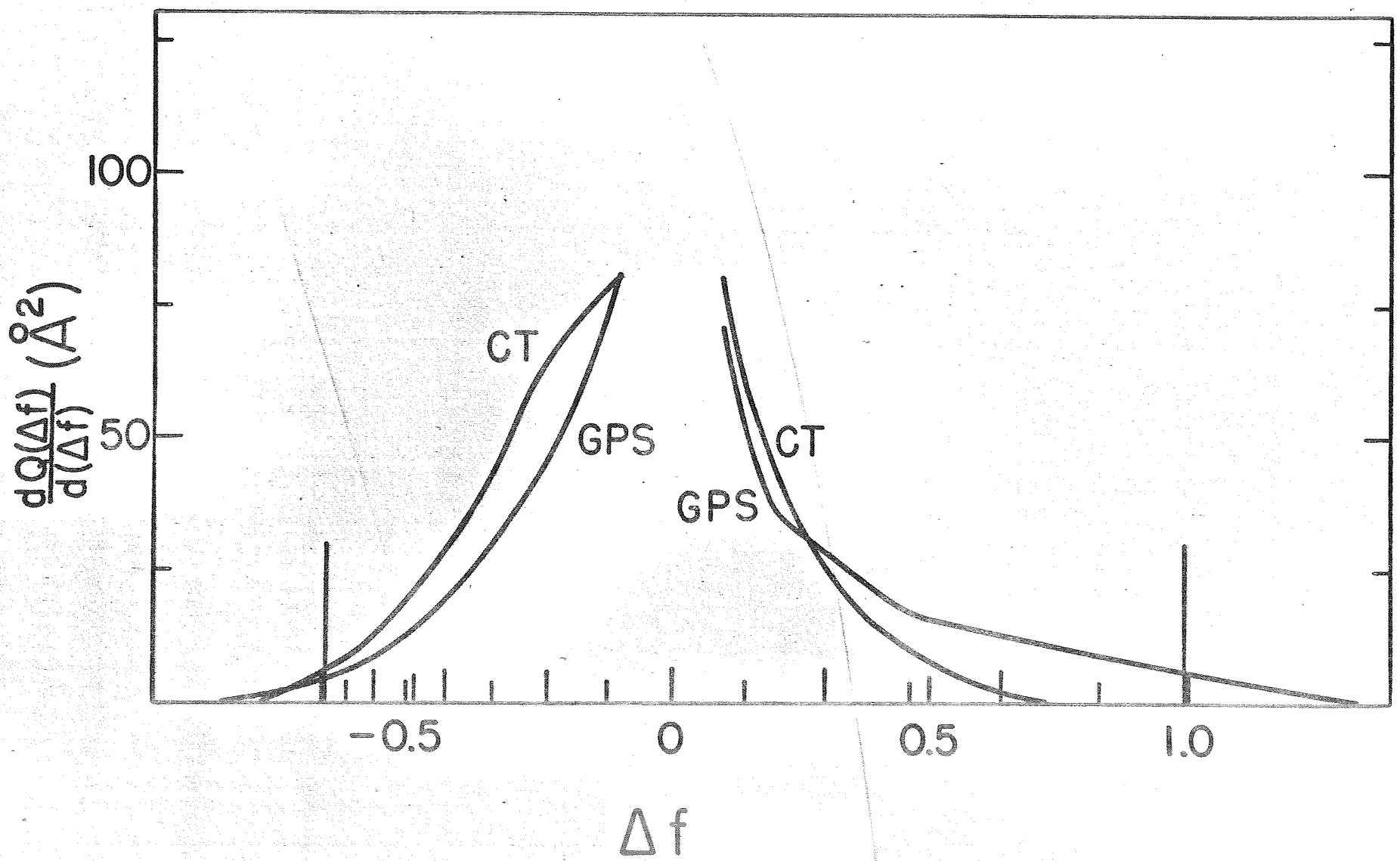

Figure 5

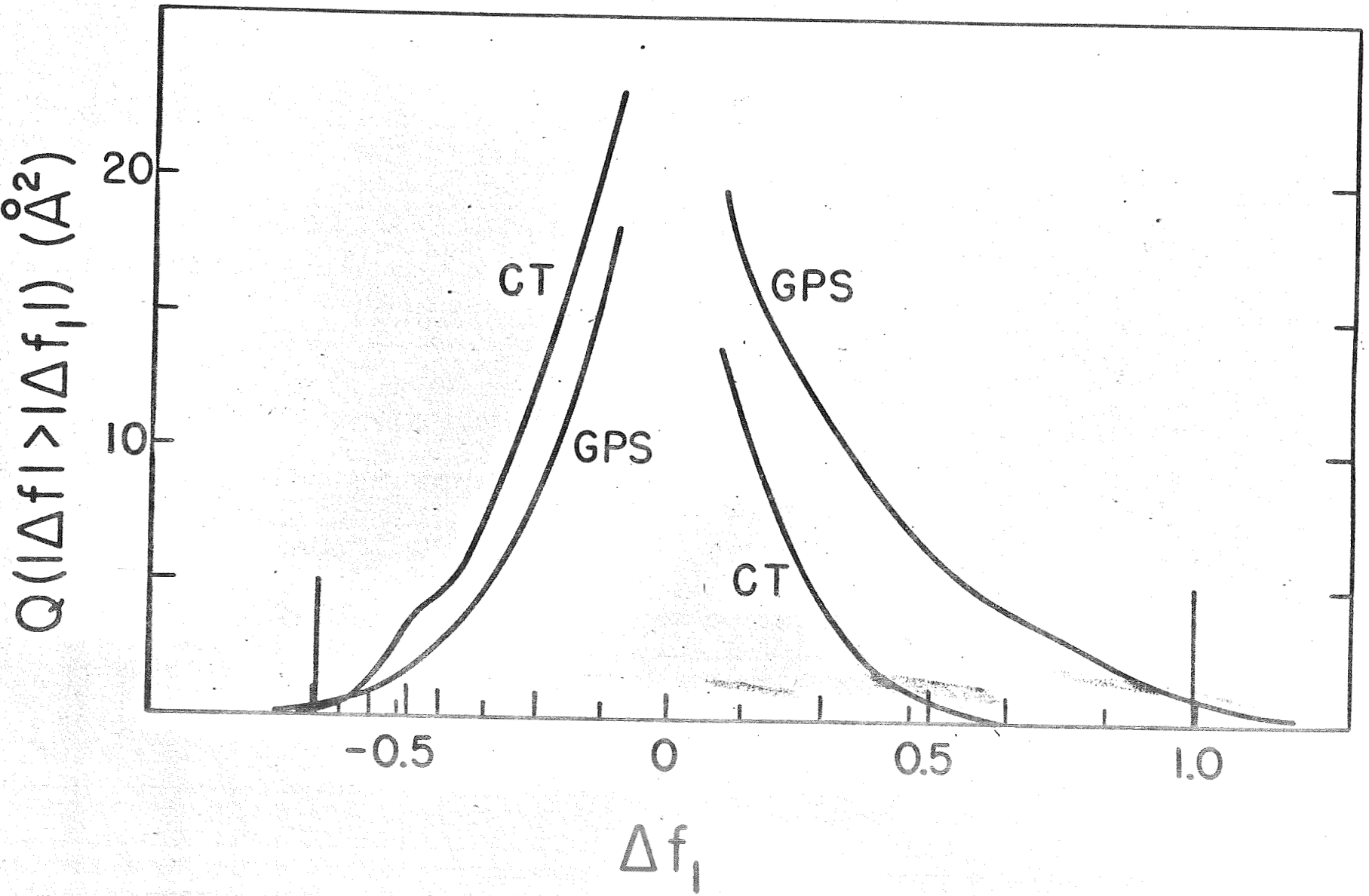

Figure 6

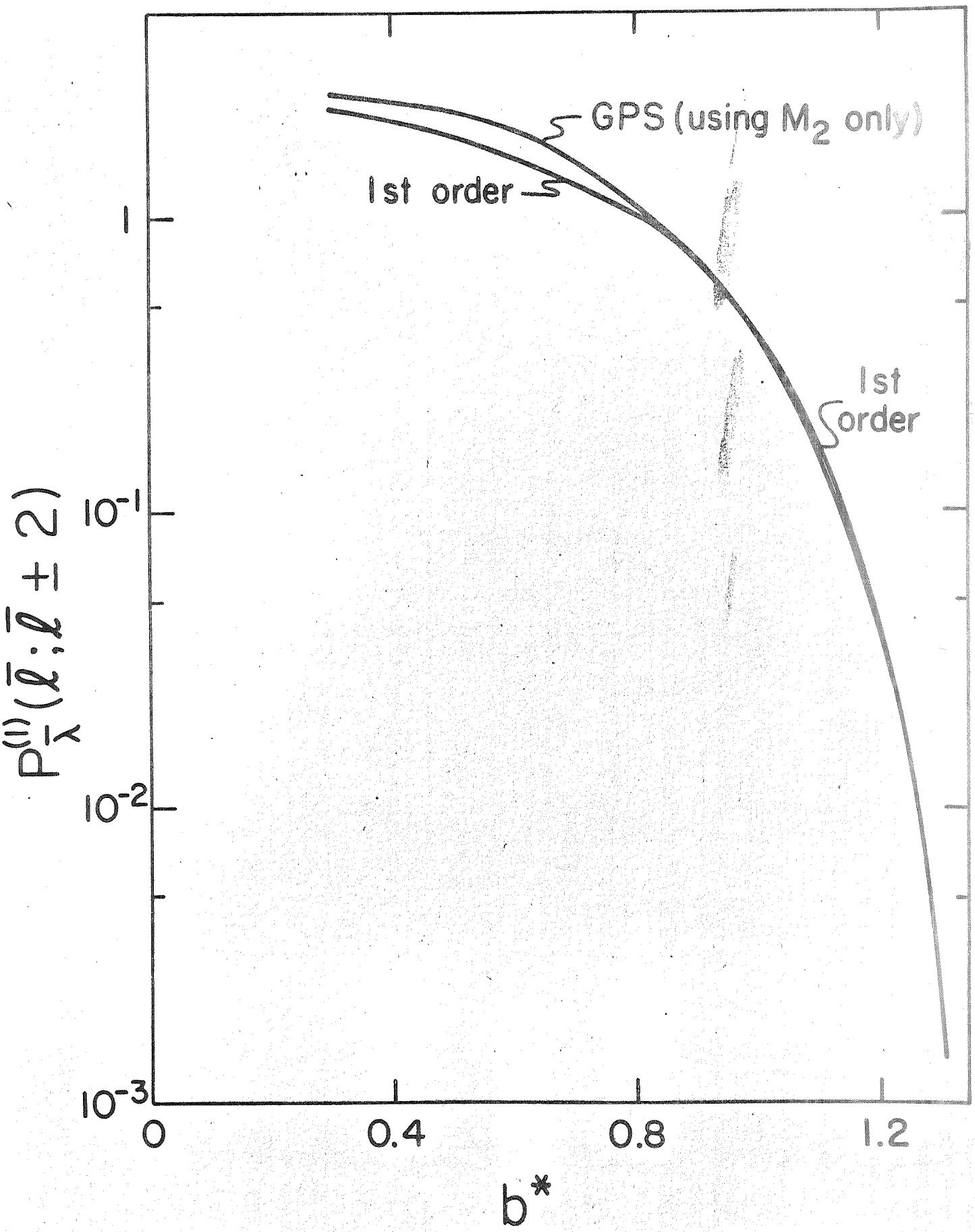
GPS (using M_2 only)
1st order
1st order
1
10^{-1}
10^{-2}
10^{-3}
$P_\lambda^{(1)}(\ell;\ell+2)$
0
0.4
0.8
1.2
b^*

Figure 7

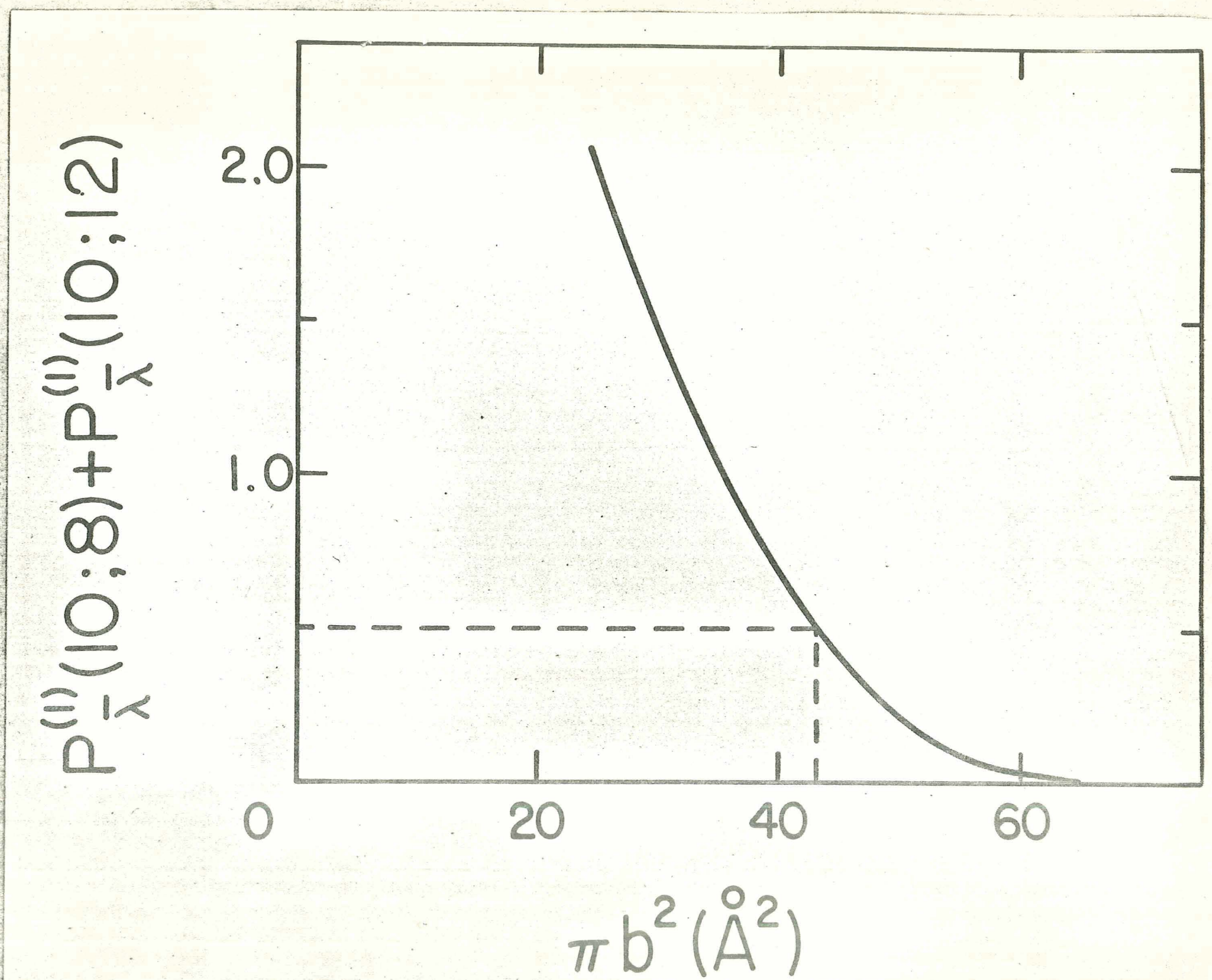
$P_{\bar{\lambda}}^{(\parallel)}(10;8)+P_{\bar{\lambda}}^{(\parallel)}(10;12)$
2.0
1.0
0
20
40
60
$\pi b^2 (\AA^2)$

Figure 8